

Article

# Hybrid Mode: Routinization of the Transition Mode as the Third Common Mode for Compound VTOL Drones

Jiahao Hu, Jingbo Wei , Kun Liu <sup>\*</sup>, Xiaobin Yu, Mingzhi Cao and Zijie Qin 

School of Aeronautics and Astronautics, Sun Yat-sen University, Shenzhen 518107, China; hujh23@mail2.sysu.edu.cn (J.H.)

\* Correspondence: liukun6@mail.sysu.edu.cn

**Abstract:** Fixed-wing Vertical Takeoff and Landing (VTOL) drones have been widely researched and applied because they combine the advantages of both rotorcraft and fixed-wing drones. However, the research on the transition mode of this type of drone has mainly focused on completing the process quickly and stably, and the application potential of this mode has not been given much attention. The objective of this paper is to routinize the transition mode of compound VTOL drones, i.e., this mode works continuously for a longer period of time as a third commonly used mode besides multi-rotor and fixed-wing modes, which is referred to as the hybrid mode. For this purpose, we perform detailed dynamics modeling of the drone in this mode and use saturated PID controllers to control the altitude, velocity, and attitude of the drone. In addition, for more stable altitude control in hybrid mode, we identify the relevant parameters for the lift of the fixed-wings and the thrust of the actuators. Simulation and experimental results show that the designed control method can effectively control the compound VTOL drone in hybrid mode. Moreover, it is proven that flight in hybrid mode can reduce the flight energy consumption to some extent.

**Keywords:** compound VTOL drone; transition mode; model identification; control strategy



**Citation:** Hu, J.; Wei, J.; Liu, K.; Yu, X.; Cao, M.; Qin, Z. Hybrid Mode: Routinization of the Transition Mode as the Third Common Mode for Compound VTOL Drones. *Drones* **2024**, *8*, 93. <https://doi.org/10.3390/drones8030093>

Academic Editor: Mostafa Hassanalian

Received: 3 February 2024

Revised: 5 March 2024

Accepted: 6 March 2024

Published: 8 March 2024



**Copyright:** © 2024 by the authors. Licensee MDPI, Basel, Switzerland. This article is an open access article distributed under the terms and conditions of the Creative Commons Attribution (CC BY) license (<https://creativecommons.org/licenses/by/4.0/>).

## 1. Introduction

Drones have generated a great deal of interest in recent years in both the military and civilian sectors because of their enormous potential for applications in reconnaissance, photography, transportation, rescue, and other areas [1]. Currently, there are two main types of common drones: fixed-wing drones and rotorcraft drones. Both types have their own advantages and limitations. Fixed-wing drones have more obvious advantages in terms of cruising speed, payload, and flight range and duration, but they are constrained by take-off and landing fields and flight velocity. Rotorcraft drones, on the other hand, have no site limitations and have hovering capability, which gives them great flexibility; however, their flight speed and range are much lower than those of fixed-wing drones [2,3]. Therefore, fixed-wing vertical take-off and landing (VTOL) drones, which combine the advantages of the two types of drones, have a wide range of development prospects and have now become a popular research topic [3–6]. Various designs have been proposed for this type of drone, commonly including tilt-rotor [7,8], tilt-wing [9,10], tail-sitter [11,12] and compound VTOL [13,14].

VTOL drones have two primary modes of flight: multi-rotor flight mode and fixed-wing flight mode. These two modes of flight are connected by a transition mode, which usually persists only for a short period of time. In terms of flight control, the difficulties of transition control for VTOL drones have long been the focus of researchers due to their high dynamic uncertainty and the serious aerodynamic interference between rotors and wings [15–23]. Yeo et al. [24] proposed a gain-scheduled altitude control method to ensure stable transitions with minimal altitude changes, and this strategy is effective in allowing drones to maintain stability and altitude accuracy in transition modes. Liu et al. [25]

designed a unified six degrees of freedom (6-DOF) nonlinear control strategy using the Incremental Nonlinear Dynamic Inversion (INDI) method for the control during transitions, which effectively manages the complex dynamics of the transition maneuvering without the need to change the control logic. Zhao et al. [26] transformed the transition strategy design problem into an optimal control problem with constraints, while the Gauss pseudospectral method (GPM) was employed to transform and solve the problem, effectively balancing the relationship between transition time, control inputs and attitude stability. Yuksek et al. [27] designed a low-altitude flight control system based on an adaptive dynamic inversion method, using reinforcement learning methods to provide safety and energy efficiency during the transition flight phase, which improves the adaptability and efficiency of transition management for drones in complex urban environments. Dickeson et al. [28] designed a robust  $H_\infty$  control method based on the conversion of a linear parameter variation model, which improves the robustness of the system under unmodeled dynamic conditions. Ye et al. [29] proposed a soft transition mode using a control law that consists of implicit nonlinear dynamic inversion (NDI) and incremental nonlinear dynamic inversion (INDI). This approach improves robustness, safety, and smoothness during transitions.

To the best of our knowledge, although there are many studies on the control of transition modes in VTOL drones, the vast majority of them only aim to complete the transition process quickly and stably, and no researcher has yet proposed the transition process as a common flight mode. However, as the missions that VTOL drones are required to perform become more complex, the drones will need to be used more frequently in low-speed flight situations, which are difficult for this type of drone to adapt to (when flying in multi-rotor mode, the drag may be too high and it may be difficult to reach the desired velocity. Conversely, when flying in fixed-wing mode, the velocity may be excessive). Therefore, we focus on the transition mode due to its suitability for low speed flight. From our perspective, routinizing the transition mode has the following potential:

1. The VTOL drones have a large portion of the flight speed envelope in between the multi-rotor and fixed-wing modes that is not being effectively utilized.
2. During transition mode, the VTOL drones can maintain a horizontal attitude at a relatively low speed without the tilting of the airframe required by rotorcraft. This feature has the potential for use in various applications, such as power system inspection, disaster search and rescue, and aerial photography.
3. Compared to rotorcraft, VTOL drones use fixed-wings to provide lift during transition mode, which reduces energy consumption to some extent.

This paper proposes the use of the transition mode of a compound VTOL drone as a third common flight mode, alongside multi-rotor and fixed-wing modes. This mode will be referred to as the hybrid mode. The main contributions of this paper are outlined below:

1. We routinize the transition mode of a compound drone (meaning that the transition mode is used as a mode that works continuously for an extended period of time), propose the hybrid mode, and design its flight logic.
2. Combining the flight characteristics of the drone in hybrid mode, we establish its 6-DOF dynamics model in detail, and completely design the corresponding control strategy and controllers.
3. A method is proposed to identify the fixed-wing lift parameters of this type of drones in hybrid mode. Conventional wind tunnel tests are particularly costly and are generally not applied to small VTOL drones for economic reasons. The proposed method can effectively reduce the cost of identifying the fixed-wing lift and can be applied to a wide range of VTOL drones.
4. The proposed flight method is verified through simulation, and a compound VTOL drone prototype is built for real flight experiments.

The remainder of this paper is structured as follows: In Section 2, the dynamic model of the system will be built. The control strategy and controllers design are overviewed

in Section 3. Simulations and experimental validation are presented in Sections 4 and 5, respectively. Finally, conclusions and future works are drawn in Section 6.

## 2. Modelling of the System

In this section, we introduce the flight control logic of the compound VTOL drone for hybrid mode, combine the motion characteristics of the drone to build its dynamic model in this particular mode, and describe the relevant parameter identification.

### 2.1. Hybrid Mode Control Logic

The power system of the drone in this work consists of two parts. One is the four multi-rotor actuators that generate vertical thrust, and the other one is the tail-thrust actuator located at the rear of the fuselage that generates forward thrust for the drone. All motor actuators are activated, and the control surfaces of the fixed-wing are made ineffective in hybrid mode.

As shown in Figure 1 the flight control logic of the compound VTOL drone for hybrid mode is designed as follows:

- Vertical motion: When the combined lift generated by the four multi-rotor actuators and the fixed-wing due to aerodynamic force is greater than the gravity of the drone, the drone ascends; otherwise, it descends. When the combined lift is equal to the drone's gravity, the drone maintains its current altitude.
- Forward motion: Compared to the multi-rotor mode, forward motion in hybrid mode is achieved by using the tail actuator to provide thrust rather than generating a specific pitch change to allow the multi-rotor actuators to provide forward thrust. In hybrid mode, the forward acceleration and deceleration of the drone are controlled by the rotational speed of the tail actuators, and the drone cannot move backward.
- Lateral motion: Similar to a quadrotor, the lateral motion of the drone is achieved by the difference in rotational speed between the left and right multi-rotor actuators, causing the fuselage to roll and thus generate lateral thrust. Taking rightward movement as an example, the rotational speed difference causes the drone to roll. At this moment, the multi-rotor actuators create a rightward thrust. Simultaneously, due to the aerodynamic force, the fixed-wing also produces a component of rightward thrust, enabling the drone's movement to the right. The leftward motion is the same.
- Yaw motion: The four multi-rotor actuators generate a gyroscopic torque when they rotate. When the rotational speed of one pair of actuators increases while that of the other pair decreases, the gyroscopic torque rotates the fuselage. The rotational direction of the drone is opposite to that of the actuators whose rotational speed increases.

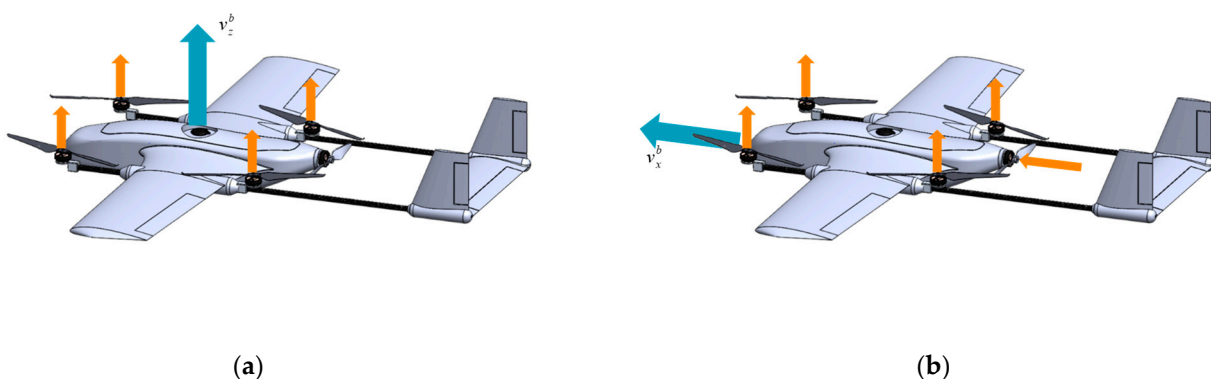
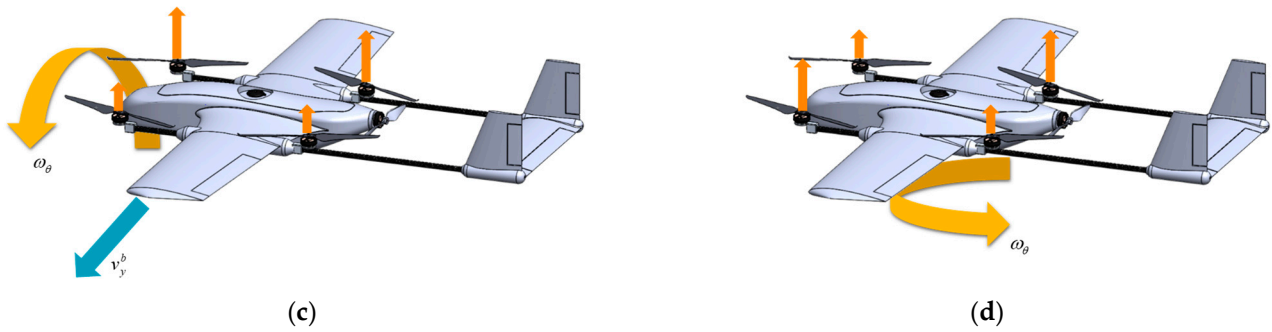


Figure 1. Cont.



**Figure 1.** Hybrid mode control logic: (a) Vertical motion; (b) Forward motion; (c) Lateral motion; (d) Yaw motion.

2.2. Dynamic Model

In the conventional transition mode, most VTOL drones only perform forward acceleration, so only the longitudinal model of the drone is usually considered [30]. However, it is necessary to build a complete dynamic model of the drone in hybrid mode.

The modeling of drones is very complicated. In order to make the model simple and without losing its relevance, we consider the drone to be a rigid body. Therefore, the state variables describing its motion can be reduced to the position and velocity in the inertial frame, as well as its attitude represented by the body frame and angular velocity.

As shown in Figure 2a, body frame ( $O_b x_b y_b z_b$ ) and North-East-Down (NED) inertial frame ( $O_w x_w y_w z_w$ ) are defined.

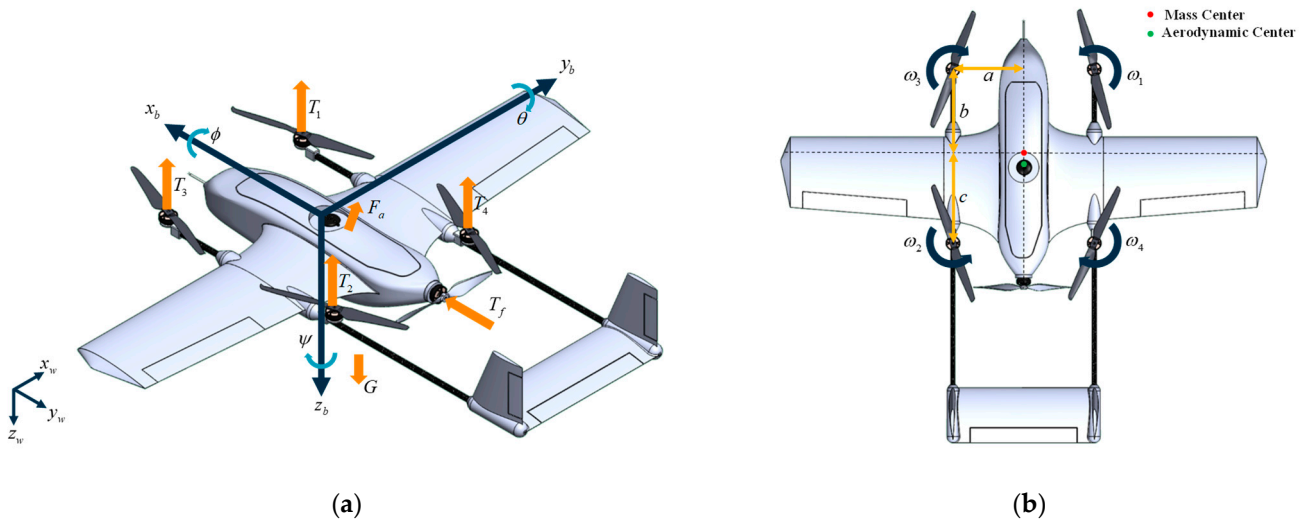


**Figure 2.** (a) Coordinate system and forces; (b) Multi-rotor actuators configuration.

2.2.1. Position Dynamics Model

According to Newton’s second law, the positional dynamic equation of the drone in the inertial frame is as follows:

$$\dot{p} = v, \tag{1}$$

$$m\dot{v} = F, \tag{2}$$

where  $m$  is the total mass of the drone,  $F$  is the resultant force,  $p$  and  $v$  are the position and velocity of the drone in the inertial frame, respectively.

The resultant force can be divided into the following parts: gravity  $G$ , collective thrust of the actuators  $T$ , aerodynamic force  $F_a$ , and disturbance force  $F_{dis}$ . Therefore, Equation (2) can be written as:

$$m\dot{v} = T + F_a + G + F_{dis}, \tag{3}$$

Since the thrust of the actuators and the aerodynamic force are more intuitive and convenient in the body frame, we can further obtain:

$$m\dot{v} = R_b^w T^b + R_b^w F_a^b + G + F_{dis}, \quad (4)$$

where  $R_b^w$  is the transformation matrix from the body frame to the inertial frame, and the superscript  $^b$  denotes the vector in the body frame.

The collective thrust includes the thrusts of the multi-rotor actuators  $T_{mc}$  and the tail-thrust actuator  $T_f$ , which can be written as:

$$T^b = T_{mc} + T_f = \begin{bmatrix} c_f \omega_f^2 & 0 & -c_{mc} \sum \omega_i^2 \end{bmatrix}^T, \quad (5)$$

where  $\omega_f$  is the rotation speed of the tail-thrust actuator,  $\omega_i$  is the rotation speed of each multi-rotor actuator,  $c_f$  is the tail-thrust actuator's thrust coefficient which is influenced by the incoming airflow, and  $c_{mc}$  is the thrust coefficient for the multi-rotor actuators. This paper considers the thrust coefficients as constants and the changes caused to the airflow effects as external disturbances.

The resultant aerodynamic force is traditionally decomposed into lift force and drag [13]. We resolve it along the body frame into a lift force perpendicular to the fuselage, a lateral force, and a drag in the opposite direction of flight, as follows:

$$F_a^b = \begin{bmatrix} -c_D \rho v_a^2 S / 2 & -c_Y \rho v_a^2 S / 2 & -c_L \rho v_a^2 S / 2 \end{bmatrix}^T, \quad (6)$$

where the  $v_a$  is the airspeed,  $\rho$  is the air density, and  $S$  is the reference area of the wing. The aerodynamic coefficients  $c_D$ ,  $c_Y$ ,  $c_L$  depend on the angle of attack  $\alpha$  and sideslip angle  $\beta$ . In this work, we ensure that the fixed-wing control surfaces of the drone remain in neutral and do not engage in the control; therefore, the aerodynamic coefficients are not affected by them.

The dynamic equation of the drone also can be described in the body frame as:

$$m\dot{v}_b = T^b + F_a^b + R_w^b G + F_{dis}^b - m R_b^w \omega_b \times v_b, \quad (7)$$

where  $v_b$  and  $\omega_b$  are the velocity and rotation angular velocity in the body frame, respectively.

### 2.2.2. Attitude Dynamics Model

We assume that the rotational inertia matrix of the drone is  $I$ . According to the moment of momentum theorem, we can obtain:

$$\tau = I\dot{\omega}, \quad (8)$$

$$\tau = \tau_T + \tau_a + \tau_{dis}, \quad (9)$$

where  $\tau$  is the resultant torque and  $\omega$  is the angular velocity in the inertial frame. According to the forces mentioned above, it can be known that the torques the drone receives include the actuators torque  $\tau_T$ , the aerodynamic torque  $\tau_a$ , and the disturbance torque  $\tau_{dis}$ .

Since the drone is symmetrical about the  $O_b x_b z_b$  plane of the body frame, its inertia matrix can be written as:

$$I = \begin{bmatrix} I_{xx} & 0 & I_{xz} \\ 0 & I_{yy} & 0 \\ I_{zx} & 0 & I_{zz} \end{bmatrix}, \quad (10)$$

Based on Coriolis' theorem, in the body frame, the dynamics model of the drone can be written as:

$$I\dot{\omega}_b = \tau_T^b + \tau_a^b + \tau_{dis}^b - \omega_b \times (I\omega_b), \quad (11)$$

The relationship between the Euler angular rate  $\dot{\Theta} = [\dot{\phi} \ \dot{\Theta} \ \dot{\psi}]^T$  and the body angular velocity is:

$$\dot{\Theta} = \begin{bmatrix} 1 & \sin \phi \tan \Theta & \cos \phi \tan \Theta \\ 0 & \cos \phi & -\sin \phi \\ 0 & \sin \phi / \tan \Theta & \cos \phi / \tan \Theta \end{bmatrix} \omega_b, \quad (12)$$

The actuators' torque includes the thrust torque and gyroscopic torque generated by the multi-rotor and tail-thrust actuators. The thrust direction of the tail-thrust actuators passes through the mass center of the drone, so the thrust torque generated by the tail-thrust actuator is equal to 0. In addition, due to the wingspan of the drone's fixed wing, its rotational inertia along the  $x_b$  is large. Therefore, we neglected the gyroscopic torque of the tail-thrust actuator. Then, the actuators' torque can be expressed as:

$$\tau_T^b = A [T_1 \ T_2 \ T_3 \ T_4]^T, \quad (13)$$

$$A = \begin{bmatrix} -a & a & -a & a \\ b & -c & b & -c \\ k & k & -k & -k \end{bmatrix}, \quad (14)$$

where  $a$ ,  $b$  and  $c$  are positive scalars characterizing the positions of the actuators with respect to the center of mass, as shown in Figure 2b,  $k$  is the reverse torque coefficient of the multi-rotor actuator, and  $T_i$  is the thrust of each multi-rotor actuator.

The aerodynamic torque can be described as:

$$\tau_a^b = [-c_l \rho v_a^2 S \bar{b} / 2 \quad -c_m \rho v_a^2 S \bar{c} / 2 \quad -c_n \rho v_a^2 S \bar{b} / 2]^T, \quad (15)$$

where  $c_l$ ,  $c_m$  and  $c_n$  are the aerodynamic torque coefficients, respectively, while  $\bar{b}$  is the wingspan and  $\bar{c}$  is the mean aerodynamic chord.

### 2.2.3. Control Effectiveness Model

From the previous two subsections, the 6-DOF dynamic model of the compound VTOL drone in hybrid mode can be represented by Equations (4) and (11). For control in all degrees of freedom, we build the control effectiveness model of the drone. The inverse process of the control effectiveness model is the control allocation.

In hybrid mode, we only use the multi-rotor actuators and the tail-thrust actuator to control the drone while keeping the fixed-wing control surfaces in neutral. The required thrust and torque are controlled by the rotation speed of the actuators.

Based on Equations (5) and (13), the following matrix expression can be obtained:

$$\begin{bmatrix} T_{mc} \\ T_f \\ \tau_x \\ \tau_y \\ \tau_z \end{bmatrix} = M \begin{bmatrix} \omega_1^2 \\ \omega_2^2 \\ \omega_3^2 \\ \omega_4^2 \\ \omega_f^2 \end{bmatrix} = \begin{bmatrix} c_{mc} & c_{mc} & c_{mc} & c_{mc} & 0 \\ 0 & 0 & 0 & 0 & c_f \\ -ac_{mc} & ac_{mc} & -ac_{mc} & ac_{mc} & 0 \\ bc_{mc} & -cc_{mc} & bc_{mc} & -cc_{mc} & 0 \\ kc_{mc} & kc_{mc} & -kc_{mc} & -kc_{mc} & 0 \end{bmatrix} \begin{bmatrix} \omega_1^2 \\ \omega_2^2 \\ \omega_3^2 \\ \omega_4^2 \\ \omega_f^2 \end{bmatrix}. \quad (16)$$

### 2.3. Model Parameters Identification

Due to the influence of aerodynamic forces, the fixed-wing will always have a lift force in hybrid mode. The multi-rotor actuators need to constantly adjust thrust output to maintain the desired altitude. Since the lift generated by the fixed-wing changes with airspeed, the collective thrust of the multi-rotor actuators also needs to be adjusted with the airspeed. In order to improve the control accuracy and response speed for altitude control, it is necessary to identify the related parameters of the fixed-wing lift and multi-rotor actuators.

We assume that the drone is in a horizontal flying attitude and ignore interference forces. Expanding Equation (4) in the  $z_w$  direction, we can obtain:

$$m\dot{v}_z = mg + T_{mc} + F_{a,z} = mg - c_{mc} \sum \omega_i^2 - \mathbb{C}_L v_a^2, \quad (17)$$

where  $c_{mc}$  and  $\mathbb{C}_L = c_L \rho S / 2$  are the unknown parameters.

Thrust throttle is often used in practice to control the collective thrust of the multi-rotor actuators. As shown in Figure 3a, each actuator consists of an ESC, a motor, and a propeller. With the throttle command  $\sigma \in [0, 1]$  and the battery voltage  $E$ , the actuators produce the collective thrust  $T_{mc}$ . Obviously, thrust and throttle are positively correlated as  $T_{mc} \propto \sigma$ , which is easily obtained from a thrust test platform.

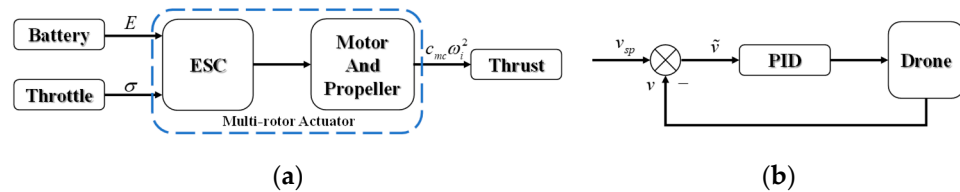


**Figure 3.** (a) The multi-rotor actuator model; (b) Velocity controller of fixed-wing lift identification.

From Equation (17), when  $\dot{v}_z = 0$  we can obtain:

$$|F_{a,z}| = \mathbb{C}_L v_a^2 = mg - |T_{mc}|. \quad (18)$$

We set the desired vertical velocity to 0 and conduct multiple flight tests at different airspeeds. We keep the desired pitch angle at 0 to avoid thrust coupling and consider both the angle of attack and sideslip angle as 0, as we will mention in the control strategy of Section 3. Then, we use a simple PID controller to control the vertical and forward velocities as shown in Figure 3b, which can be described as:

$$u = k_{v,p} \tilde{v} + k_{v,i} \int \tilde{v} dt + k_{v,d} \tilde{v} / dt. \quad (19)$$

When the height and forward velocity of the drone stabilize, throttle  $\sigma$  can be obtained from the autopilot. From Equation (18), we can compute the parameter  $\mathbb{C}_L$ .

The identification result will be shown in Section 5.

### 3. Control Strategy and Controllers Design

This section first introduces the control strategy of the drone in the hybrid mode, and then details the design of the controllers.

#### 3.1. Hybrid Mode Control Strategy

As mentioned in the control logic, in hybrid mode, only the multi-rotor actuators and the tail-thrust actuator are involved in the control of the drone, while the fixed-wing control surfaces are not activated in order to avoid control coupling. The fixed-wing acts as part of the lift generation, and the multi-rotor actuators supplement the lift for maintaining altitude.

In this mode, we adopt a control strategy similar to that of a rotorcraft. Except for the forward velocity, which is controlled through the tail-thrust actuator, the motion of the drone is mainly controlled by the four multi-rotor actuators. Therefore, to facilitate the subsequent controller design, we simplify the dynamics model in Section 2.

We consider aerodynamic forces and torques, other than aerodynamic lift in the direction of the  $z_b$ , as external disturbances and incorporate them into the disturbance term. Then, Equations (4) and (11) can be written as:

$$m\dot{v}_w = \mathbf{R}_b^w \mathbf{T}^b + \mathbf{R}_b^w \mathbf{L}^b + \mathbf{G} + \mathbf{F}_{dis}, \quad (20)$$

$$I\dot{\omega}_b = \tau_T^b + \tau_{dis}^b - \omega_b \times (I\omega_b), \tag{21}$$

where  $L^b = [0 \ 0 \ -c_L\rho v_a^2 S/2]^T$  is the lift represented in the body frame.

Afterward, in hybrid mode, we adopt a hierarchical control architecture that includes external loops (called position controller) and internal control loops (called attitude controller), as shown in Figure 4.

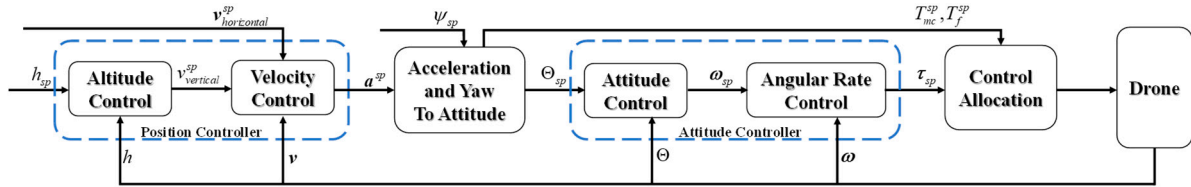


Figure 4. Control Architecture.

In the position controller (Figure 5a), in the vertical direction, we design the controller with feedforward, and in the horizontal direction we transform the coordinate frame into the heading frame for the controller design. The attitude controller (Figure 5b) we designed is the same as in a common rotorcraft. However, we expect the pitch angle to always be set to 0 to keep the drone’s lift relatively stable.

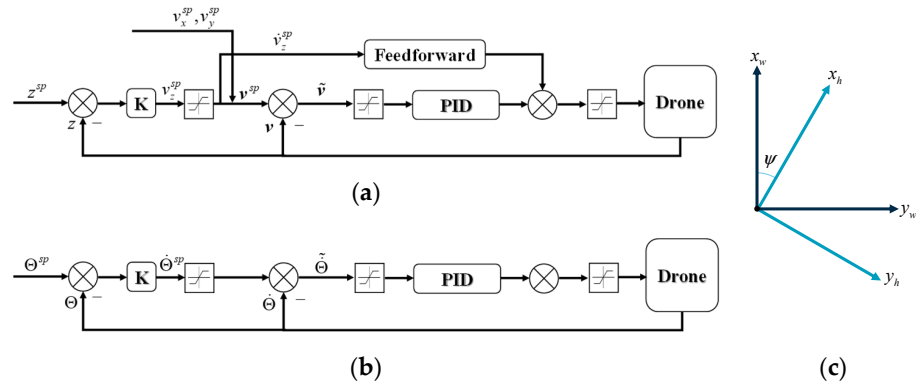


Figure 5. (a) Position controller architecture; (b) Attitude controller architecture; (c)Heading frame.

It is worth mentioning that there is always a slow time-varying disturbance due to aerodynamic forces in the disturbance term in Equations (20) and (21), and since the controllers we designed are basically PID controllers, we need to consider anti-saturation for the integral term.

The detailed design of the controller is described in the following subsections.

### 3.2. Position Controller

We separate the position control problem into vertical altitude control and horizontal control. Since the drone has forward velocity at all times in hybrid mode, we disengage the horizontal position control and preserve the control of altitude. In horizontal control, only velocity control is available.

#### 3.2.1. Altitude Control

The objective of the altitude control module is to define a desired vertical speed  $v_z^{sp}$  as an intermediate variable, as well as to control the height error and keep it converging to 0.

Define the saturation equation as:

$$Sat_{x_{min}}^{x_{max}} | x = \begin{cases} x^{\min} & (x < x^{\min}) \\ x & (x^{\min} \leq x \leq x^{\max}) \\ x^{\max} & (x > x^{\max}) \end{cases}. \tag{22}$$

We propose the following saturated proportional controller:

$$v_z^{sp} = Sat_{v_z^{\min}}^{v_z^{\max}} |k_z(z - z^{sp}), \quad (23)$$

where  $k_z$  is the proportional control coefficient,  $z$  and  $z^{sp}$  are the current and desired heights, respectively. With a North-East-Down convention for the inertial frame,  $|v_z^{\min}|$  is the maximum climbing velocity and  $v_z^{\max}$  is the maximum descending velocity.

In order to achieve the convergence of the vertical velocity  $v_z$  to the setpoint  $v_z^{sp}$ , we need to obtain the desired vertical acceleration  $a_z^{sp}$ . We propose the following PID controller with feed forward as:

$$\tilde{v}_z = v_z - v_z^{sp}, \quad (24)$$

$$a_z^{sp} = Sat_{a_z^{\min}}^{a_z^{\max}} \left| -k_{vz}^P \tilde{v}_z - k_{vz}^I I_{vz} + k_{vz}^D \dot{\tilde{v}}_z + k_f \dot{v}_z^{sp} \right., \quad (25)$$

$$I_{vz} = \begin{cases} 0 & (|I_{vz}| \geq I_{vz}^m) \text{ and } (I_{vz} \tilde{v}_z > 0) \\ Sat_{-I_{vz}^m}^{I_{vz}^m} \int \tilde{v}_z dt & \text{otherwise} \end{cases}, \quad (26)$$

where  $k_{vz}^P$ ,  $k_{vz}^I$  and  $k_{vz}^D$  are positive proportional, integral and differential gains, respectively, while  $a_z^{\max}$  and  $a_z^{\min}$  are the vertical acceleration constraints,  $I_{vz}$  is the integral term and  $I_{vz}^m$  is its saturation value, and  $k_f$  is the feedforward gain.

### 3.2.2. Horizontal Velocity Control

Because the forward velocity control and lateral velocity control of the drone use different control actuators, we design the horizontal velocity controller in the heading frame ( $O_h x_h y_h z_h$ ) as shown in Figure 5c, where  $z_w$  and  $z_h$  coincide.

The horizontal velocity in the heading frame is:

$$v^h = [v_x \cos \psi + v_y \sin \psi, -v_x \sin \psi + v_y \cos \psi]^T. \quad (27)$$

To obtain the desired horizontal acceleration  $a_{xy}^{h,sp}$ , we design the PID controller for horizontal velocity as follows:

$$\tilde{v}^h = v^h - v^{h,sp}, \quad (28)$$

$$a_{xy}^{h,sp} = Sat_{a_{h,\min}}^{a_{h,\max}} \left| -k_v^P \tilde{v}^h - k_v^I I_v + k_v^D \dot{\tilde{v}}^h \right., \quad (29)$$

$$I_v = \begin{cases} 0 & (|I_v| \geq I_v^m) \text{ and } (I_v \tilde{v}^h > 0) \\ Sat_{-I_v^m}^{I_v^m} \int \tilde{v}^h dt & \text{otherwise} \end{cases}, \quad (30)$$

where  $k_v^P$ ,  $k_v^I$  and  $k_v^D$  are PID gains,  $a^{h,\max}$  and  $a^{h,\min}$  are the horizontal acceleration constraints,  $I_v$  is the integral term and  $I_v^m$  is its saturation value.

In the control of forward velocity, we consider the influence of aerodynamic force, and thus focus on controlling the airspeed  $v_a$ . Therefore, we modify  $v^h$  in Equation (29) to be:

$$v^h = [v_a, -v_x \sin \psi + v_y \cos \psi]^T, \quad (31)$$

### 3.3. Thrust and Attitude Setpoints Calculation

#### 3.3.1. Thrust

The calculation of thrust is divided into two parts. One is the forward thrust, which is derived from the forward acceleration performed by the tail-thrust actuator, and the remaining acceleration component is provided by the multi-rotor actuators.

The forward thrust can be easily obtained as:

$$T_x^h = Sat_0^{T_x^{h,\max}} |k_{thr} a_x^{h,sp}, \quad (32)$$

where is  $k_{thr}$  forward thrust factor. Because the desired pitch angle is equal to 0, we assume that the change in pitch angle is small, so the tail thrust is equal to the forward thrust  $T_f = T_x^h$ .

In order to calculate the desired collective thrust of the multi-rotor actuators, we first compute the hover thrust obtained from lift identification as:

$$T_{hover} = -mg / \cos \phi \cos \Theta - L_{ide} \quad (33)$$

where  $L_{ide}$  is the fixed-wing lift obtained from the identification.

Then, we can observe the actuators' vertical thrust as:

$$T_z = ma_z + T_{hover} \cos \phi \cos \Theta. \quad (34)$$

If we define the total desired acceleration vector as  $\mathbf{a}^{h,sp}$ , then we can calculate the multi-rotor collective thrust as:

$$T_{mc} = T_z \frac{|\mathbf{a}^{h,sp} - a_x^h \mathbf{x}_h|}{(\mathbf{a}^{h,sp} - a_x^h \mathbf{x}_h) \cdot \mathbf{z}_h}. \quad (35)$$

### 3.3.2. Attitude Setpoints

As mentioned above, the desired pitch angle is always set to 0, the desired yaw angle is entered externally, and only the desired roll angle needs to be calculated.

The desired attitude is computed from the rotation matrix based on the vector of the desired  $\mathbf{z}_b$ . The direction of  $\mathbf{z}_b$  is the same as the direction of the collective thrust from the rotor actuator, which can be described as:

$$\mathbf{z}_b^w = \mathbf{R}_h^w \frac{(\mathbf{a}^{h,sp} - a_x^h \mathbf{x}_h)}{|\mathbf{a}^{h,sp} - a_x^h \mathbf{x}_h|}, \quad (36)$$

where  $\mathbf{z}_b^w$  represents that  $\mathbf{z}_b$  is expressed in the inertial frame.

Since the desired pitch angle is 0 and the direction of  $\mathbf{x}_b^w$  is in the  $(\mathbf{O}_w \mathbf{x}_w \mathbf{y}_w)$  plane, it can be written as:

$$\mathbf{x}_b^w = [\cos \psi^{sp} \quad \sin \psi^{sp} \quad 0]^T. \quad (37)$$

From  $\mathbf{z}_b^w$  and  $\mathbf{x}_b^w$  we can obtain:

$$\mathbf{y}_b^w = \mathbf{z}_b^w \times \mathbf{x}_b^w. \quad (38)$$

By the rotation matrix from the body frame to the inertial frame  $\mathbf{R}_b^w$  we can obtain:

$$y_{b,z}^w = \sin \phi^{sp} \cos \Theta^{sp}. \quad (39)$$

Since  $\Theta^{sp} = 0^\circ$ , we can calculate:

$$\phi^{sp} = \arcsin y_{b,z}^w. \quad (40)$$

### 3.4. Attitude Controller

The design of the attitude controller is the same as that of an ordinary rotorcraft. As shown in Figure 5b, the center of mass and the aerodynamic center of the drone do not coincide. This results in the drone always being disturbed by the aerodynamic torque, which easily causes the integration saturation. For this reason, we designed a saturated cascade PID controller as follows:

$$\dot{\Theta}^{sp} = \text{Sat}_{-\dot{\Theta}^m}^{\dot{\Theta}^m} |k_{\dot{\Theta}} (\Theta - \Theta^{sp})|, \quad (41)$$

$$\tilde{\Theta} = \dot{\Theta} - \dot{\Theta}^{sp}, \quad (42)$$

$$\ddot{\Theta}^{sp} = \text{Sat}_{-\ddot{\Theta}^m}^{\ddot{\Theta}^m} \left| -k_{\Theta}^P \tilde{\Theta} - k_{\Theta}^I I_{\Theta} + k_{\Theta}^D \dot{\tilde{\Theta}} \right., \quad (43)$$

$$I_{\Theta} = \begin{cases} 0 & \left( |I_{\Theta}| \geq I_{\Theta}^m \right) \text{ and } \left( I_{\Theta} \dot{\tilde{\Theta}} > 0 \right), \\ \text{Sat}_{-I_{\Theta}^m}^{I_{\Theta}^m} \int \tilde{\Theta} dt & \text{otherwise} \end{cases}, \quad (44)$$

where  $k_{\Theta}$  is the angle proportional gain, while  $k_{\Theta}^P$ ,  $k_{\Theta}^I$  and  $k_{\Theta}^D$  are the angular rate PID gains and  $I_{\Theta}$  is the integral term.

We then obtain the desired torque  $\tau_T^b$  from Equations (12) and (21). Finally, we pseudo-inverse  $M$  in Equation (16) to obtain the control allocation matrix, and then we can obtain the target rotation speed of each actuator.

#### 4. Simulations

To verify the feasibility of the above control strategy and designed controllers, we perform numerical simulation tests in this section.

##### 4.1. Simulation Setup

The simulation tests are carried out with the Gazebo platform in conjunction with the PX4 firmware (Figure 6). Gazebo is a powerful simulation tool for robotics that can model complex environments and physical interactions. The flight control algorithms and state estimation of the drone are implemented using PX4. The two communicate with each other using the MAVLink messaging protocol. A 3D model of a compound VTOL drone is constructed, and its dynamics and aerodynamic characteristics are established. The drone model is then added to the Gazebo environment, and PX4 is used to control it.

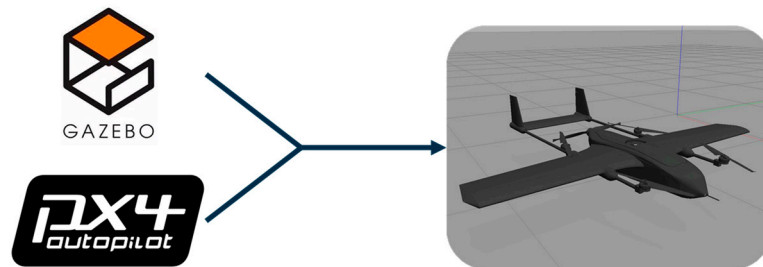


Figure 6. Simulation platform.

##### 4.2. Simulation Cases and Results

We simulated each motion state of the drone in hybrid mode as follows:

###### Case 1: Forward Motion

We let the drone accelerate to the desired airspeed, keeping it flying horizontally in this case (the simulation results are shown in Figure 7). From the results, we conclude that the drone can accelerate to and maintain the desired forward velocity in hybrid mode with a stable altitude and attitude. As flight velocity increases, the lift generated by the fixed-wing also increases. Consequently, the throttle of the multi-rotor actuators decreases to maintain altitude.

###### Case 2: Vertical Motion

In this case, we let the drone maintain a forward velocity and, at the same time, make it undergo vertical speed changes. The simulation results shown in Figure 8 indicate that vertical velocity tracking is feasible in hybrid mode, while forward flight velocity and attitude stabilization can be maintained. During vertical velocity changes, the attitude angles of the drone are slightly perturbed, but the effect is minimal.

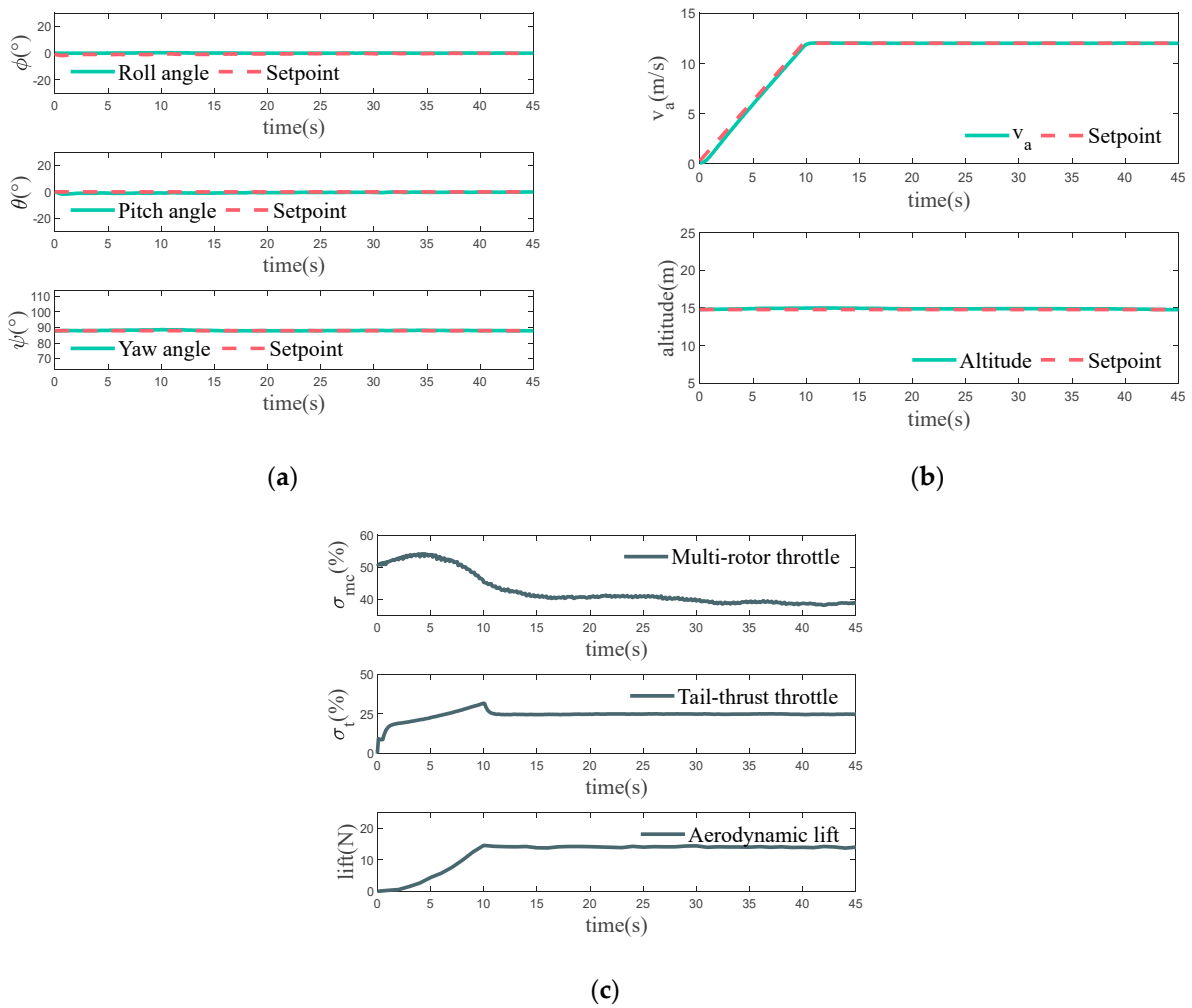


Figure 7. Simulation results for Case 1: (a) Attitude; (b) Airspeed and altitude; (c) Multi-rotor throttle, tail-thrust throttle, and aerodynamic lift.

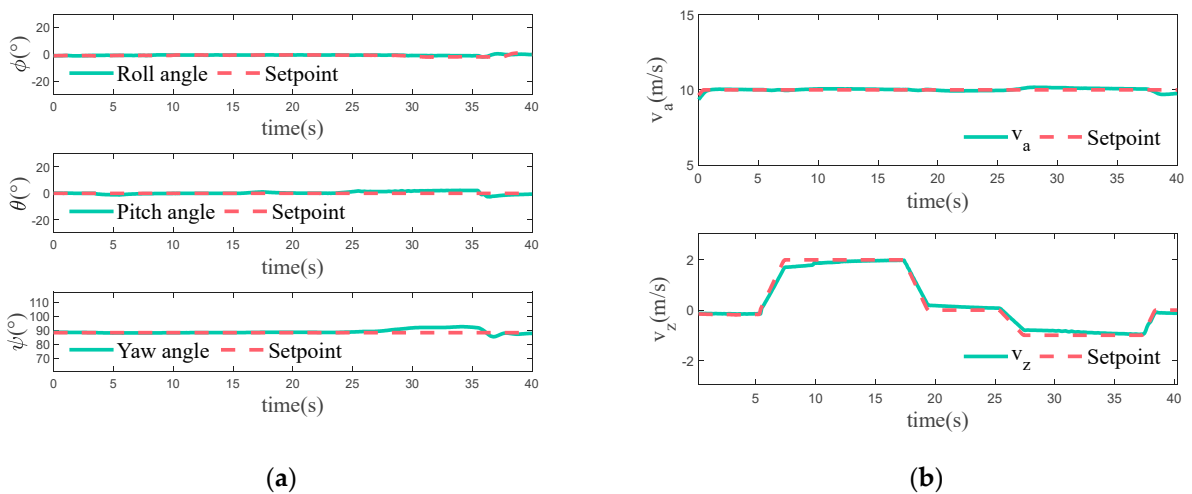
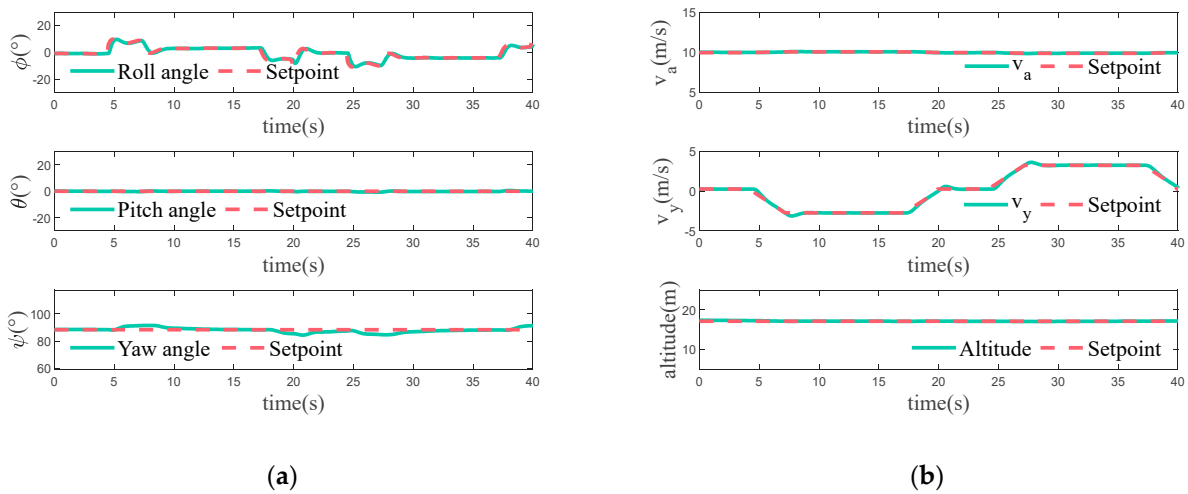


Figure 8. Simulation results for Case 2: (a) Attitude; (b) Airspeed and vertical velocity.

Case 3: Lateral Motion

In this case, we input the desired lateral velocity to cause the drone to move sideways while maintaining forward velocity. Figure 9 shows the simulation results of this case, from which it can be seen that the drone is able to control the lateral motion speed by varying the

desired roll angle, and is also capable of maintaining forward flight velocity and altitude stability. In this process, the roll angle remains fairly constant, and the yaw angle produces a small error due to disturbances.



**Figure 9.** Simulation results for Case 3: (a) Attitude; (b) Airspeed, lateral velocity, and altitude.

#### Case 4: Yaw Motion

The expectation is that the yaw angle will change in the course of maintaining a forward flight speed in this case. In the simulation results shown in Figure 10, we can see that the yaw angle can accurately follow changes in the desired yaw and remain stable in forward flight speed and altitude. Because the roll and yaw characteristics are coupled with each other, changing the yaw affects the desired roll angle. Due to the coupling of the control and disturbance, the pitch angle shows a more obvious error but remains stable overall.

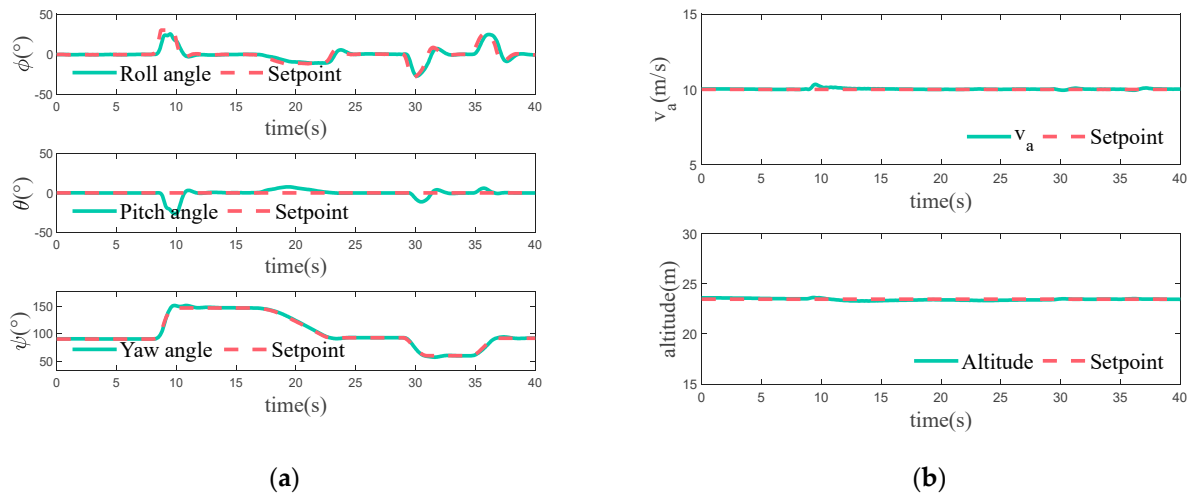


**Figure 10.** Simulation results for Case 4: (a) Attitude; (b) Airspeed and altitude.

From the above simulation results, it can be seen that it is feasible to realize the flight of the drone in hybrid mode with the designed control strategy and controllers.

## 5. Experiments

In this section, we describe a series of related experiments carried out for flight characterization of the compound VTOL drone in hybrid mode, as well as to validate the real flight performance of the designed control method.

### 5.1. Experiments Setup

As shown in Figure 11a, a prototype VTOL drone is built for the following experiments. The fuselage of the drone is a VTBIRD composite frame. The multi-rotor actuators utilize T-motor F100 (2810) KV1100 motors, T-motor FPV 45A ESC, and HQ Prop 8045 propellers. The tail-thrust actuator is composed of a Dualsky XM2838EA KV600 motor, a HobbyWing SkyWalker 80A ESC, and a SAIL 12\*6 propeller. A HOLYBRO Pixhawk V4 is used as the flight controller with PX4 v1.11 firmware [31]. Sensors include a Holybro M9N GPS and a CUAV V5 digital airspeed meter. A 6S 8000 mAh 25C LIPO battery is used as an energy source. The related technical parameters of the prototype are shown in Table 1.

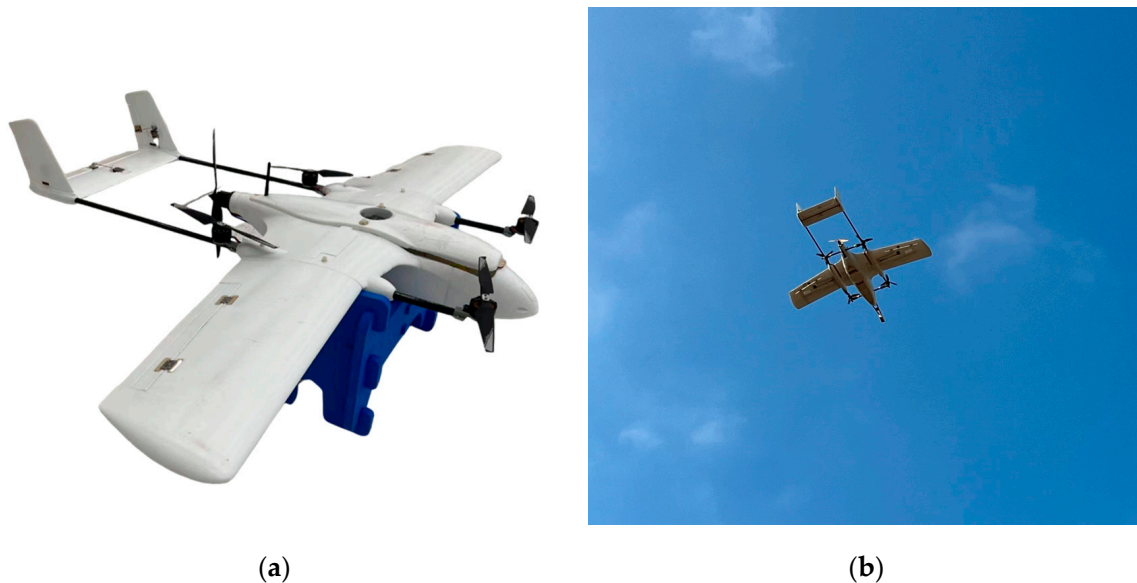


**Figure 11.** (a) Compound VTOL drone prototype; (b) Real flight experiment.

**Table 1.** Prototype related parameters.

Parameters	Value
Wingspan	1600 mm
Wing area	0.4 m <sup>2</sup>
Total weight	5.5 kg
Length	1325 m
Cruising speed	12~15 m/s
Wing incidence angle	0 degree
a *	225 mm
b *	235 mm
c *	320 mm

\* Multi-rotor actuators mounting position parameters shown in Figure 2b.

### 5.2. Parameters Identification Experiment

#### 5.2.1. Multi-Rotor Actuator Identification

To identify the multi-rotor actuator model, the thrust test platform is adopted as shown in Figure 12a.

Under the same experimental conditions, different throttle commands are given in the range [0, 1], and the results are recorded when the actuator reaches a steady state. Using the MATLAB Toolbox [32] to fit the experimental data, the identification results can be obtained, as shown in Figure 12b.

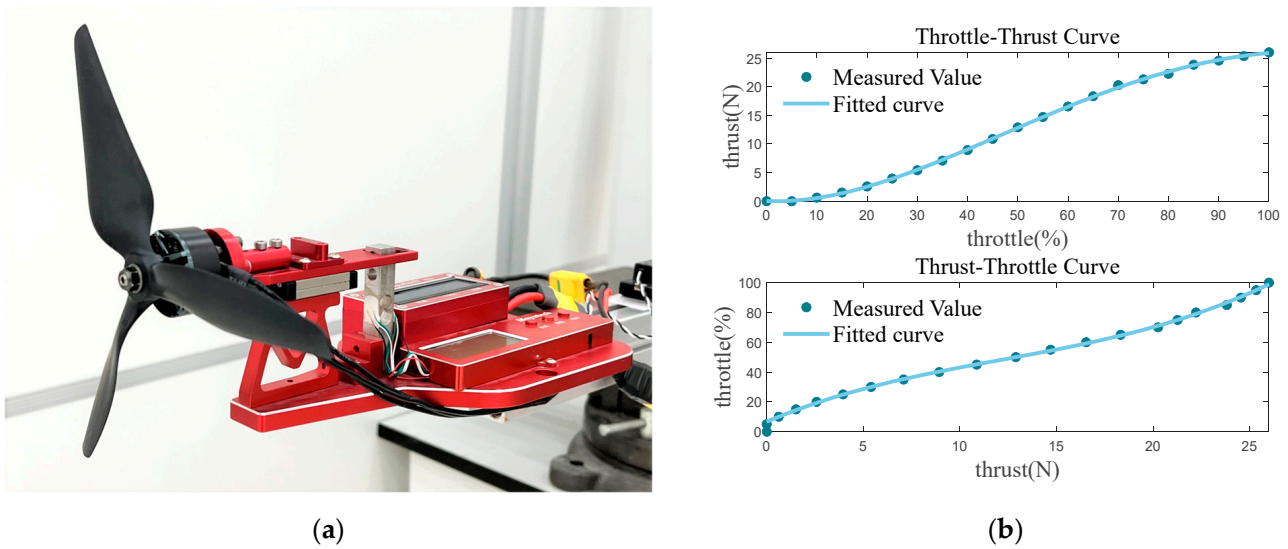


Figure 12. (a) Thrust test platform; (b) Identification results of actuator model.

From the result, it is relatively obvious that the throttle and thrust present a better relationship as a quadratic polynomial, which can be expressed as:

$$T_i = p_1\sigma_i^4 + p_2\sigma_i^3 + p_3\sigma_i^2 + p_4\sigma_i + p_5, \quad (45)$$

where  $p_1 = 22.39$ ,  $p_2 = -88.4$ ,  $p_3 = 97.51$ ,  $p_4 = -3.636$ ,  $p_5 = 0.02482$ .

In practical control, we need the output throttle to control the actuators, so we also fit the equation to obtain the throttle from the thrust as:

$$\sigma_i = q_1T_i^4 + q_2T_i^3 + q_3T_i^2 + q_4T_i + q_5, \quad (46)$$

where  $q_1 = -6.866 \times 10^{-8}$ ,  $q_2 = 7.219 \times 10^{-5}$ ,  $q_3 = -0.002581$ ,  $q_4 = 0.05502$ ,  $q_5 = 0.06689$ .

### 5.2.2. Fixed-Wing Lift Identification

We use the method described in Section 2.3 to identify the lift of the fixed-wing. The desired airspeeds from 0 to 9 m/s are divided into ten groups, with one identification group set up at 1 m/s intervals, and the experiment is repeated five times for each group of airspeeds. A total of 0 m/s can be read directly from the current hovering throttle. When the forward velocity and altitude are stabilized, the throttle of the multi-rotor actuators at that moment can be obtained. Then, the current fixed-wing lift can be calculated from Equations (18) and (46). We averaged the results of the repeated experiments for each group to get the lift of the fixed-wing at that airspeed. It should be noted that the identification experiments are conducted in nearly windless weather conditions. Therefore, it is assumed that the direction of airflow during flight is parallel to the drone's flight direction. When acquiring the throttle, we ensure that the pitch angle of the drone is stabilized at 0 degrees, so the lift obtained from the identification is the lift of the drone when flying at 0 degrees of angle of attack.

Lift is related to airspeed as a quadratic polynomial, and we express the relationship as:

$$L = r_1v_a^2 + r_2v_a + r_3. \quad (47)$$

Fitting by the MATLAB Toolbox resulted in  $r_1 = 0.6818$ ,  $r_2 = -1.543$ ,  $r_3 = -0.1112$ , and the fitting result is shown in Figure 13a.

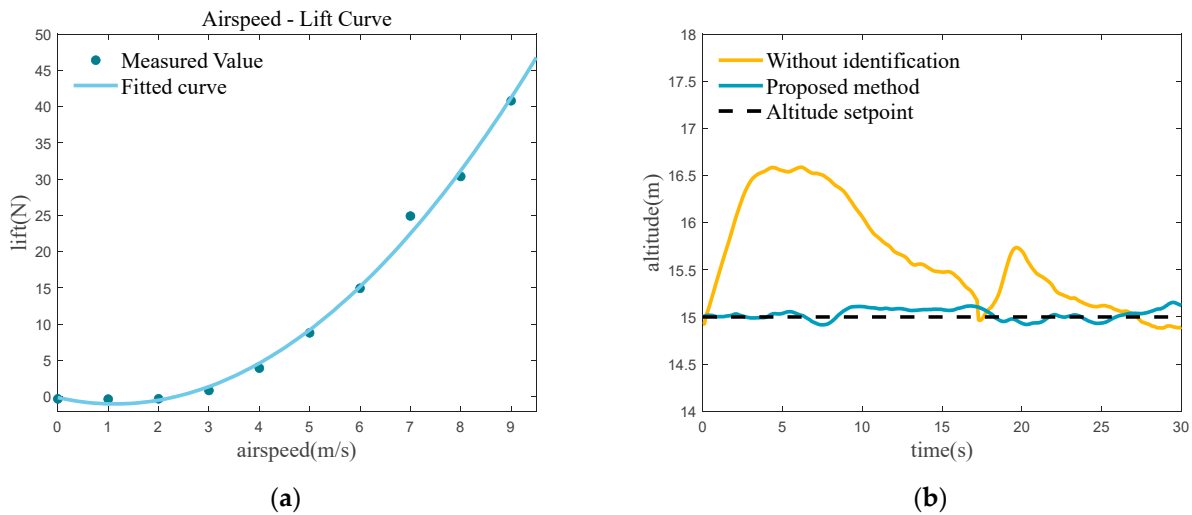


**Figure 13.** (a) Identification result of fixed-wing lift; (b) Example of height control result.

From the results, it can be seen that, when the airspeed is less than 2 m/s, the fixed-wing produces almost no lift, and, at this point, it is sufficient to fly in multi-rotor mode. When the airspeed reaches 9 m/s, the throttle of the rotor actuator is reduced to less than 25%. To ensure the control margin of the drone, 9 m/s is the maximum forward flight velocity of this drone in hybrid mode. When the required flight velocity exceeds this velocity, the drone accelerates to reach the fixed-wing cruise velocity to switch to fixed-wing mode. Therefore, we define the forward flight velocity envelope for this drone in hybrid mode as 2–9 m/s.

With the identified lift, we can accurately calculate the required thrust compensation in the vertical direction for more stable altitude control. If the lift of the fixed-wing is not included in the calculation of the required thrust for the multi-rotor actuators, and the required hovering thrust is assumed to be essentially constant (similar to that of an ordinary rotorcraft), the vertical thrust control can only be provided through the PID controller output. This will result in a slow response and large errors in altitude control.

As shown in Table 2, under the same conditions, the data obtained from the identification are included in the calculation of the vertical thrust, which reduces the maximum altitude error from 2.15 m to 0.96 m and the average error from 1.04 m to 0.06 m. Figure 13b shows an example set of experimental comparisons under the same conditions. It can be clearly seen that using the proposed method makes the height control more stable and the error smaller. Without lift identification, the fixed-wing lift initially continues to increase as the drone accelerates forward, but the multi-rotor actuators’ thrust is not reduced in time. This results in the drone being unable to maintain the desired altitude, leading to unintended climbing. As the forward velocity stabilizes, the altitude controller gradually restores the drone to the desired altitude. Furthermore, the drone’s altitude is vulnerable to change if disturbed by airflow. When the identified lift is added to the thrust calculation, the altitude control exhibits a satisfying effect.

**Table 2.** Altitude error.

	Average Error	Maximum Error
Without identification	1.04 m	2.15 m
Proposed method	0.06 m	0.96 m

### 5.3. Enhancement of Yaw Torque

In actual flight, the drone may experience significant yaw disturbances in hybrid mode due to aerodynamic forces. Since the fixed-wing rudder is not activated, yaw control relies

solely on the counter-torque generated by the rotational speed differences among the multi-rotor actuators, leading to limited control efficiency and a tendency for actuator saturation.

To address this issue in the actual flight of the prototype, we angled the multi-rotor actuators outward slightly, ensuring that the central axis of each actuator is not parallel to the  $z_b$  axis, as illustrated in Figure 14a. Consequently, the thrust component of the actuators generates torque around the  $z_b$  axis, and the differences in rotational speed among the actuators can more effectively produce the yaw control moment, enhancing the yaw angle control efficiency and disturbance resistance. This approach is widely adopted in rotorcraft design.

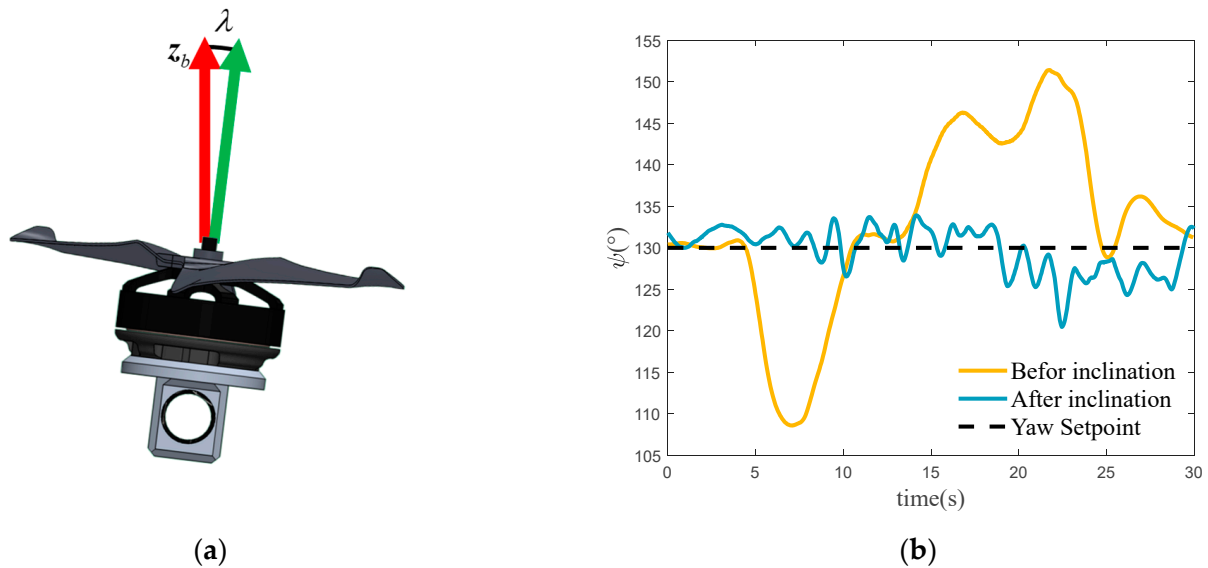


**Figure 14.** (a) Multi-rotor actuator inclination; (b) Example of enhanced yaw torque result.

For convenience, the tilt angle is set to 7 degrees. Subsequent flight tests under consistent experimental conditions showed a significant reduction in yaw angle error. As shown in Figure 14b, one test conducted at a forward velocity of 5 m/s serves as an example. With the actuators mounted vertically, the maximum error reaches 21.4 degrees, and the average error is 8.5 degrees. After tilting the actuators outward, the maximum error is reduced to 9.5 degrees, and the average error to 2.3 degrees.

#### 5.4. Real Flight Experiments

Since the aerodynamic model in the simulation environment described in Section 4 is idealized, the aerodynamic disturbances encountered during actual flight are significantly more severe and unpredictable. To evaluate the real flight performance of the drone in hybrid mode, we replicate the experiments conducted in the simulation.

##### Case 1: Forward Motion

The drone is scheduled to gradually accelerate to the desired velocity and maintain horizontal flight in this case. According to the experimental results shown in Figure 15, the drone is capable of accelerating to the desired velocity and maintaining a stable speed while keeping the altitude basically constant. Since the tail-thrust actuator has a practical response time, there is a delay of approximately 1 s during acceleration. During the first 5 s, the drone experiences slight fluctuations in attitude angles, especially in the yaw angle. These fluctuations are caused by the significant changes in aerodynamic forces during this time. The variation in the desired roll angle is due to the need for the drone to maintain a constant lateral velocity due to airflow disturbances. As the velocity stabilizes, the attitude angle also stabilizes. Furthermore, the increase in velocity results in an increase in fixed-wing lift, leading to a decrease in throttle output from the multi-rotor actuators. In an undisturbed environment, the multi-rotor actuators' throttle is 50% when the drone is

hovering. In the event of disturbance, the actuators need to be supplemented with some throttle to maintain altitude control and flight stability. In this case, when the velocity of the drone is low during acceleration, the lift provided by the fixed-wing is not significant, but the disturbance is relatively large, so there is a situation where the throttle of the multi-rotor actuators is increased. Only when a certain velocity is reached does the throttle of the multi-rotor actuators show a noticeable drop.

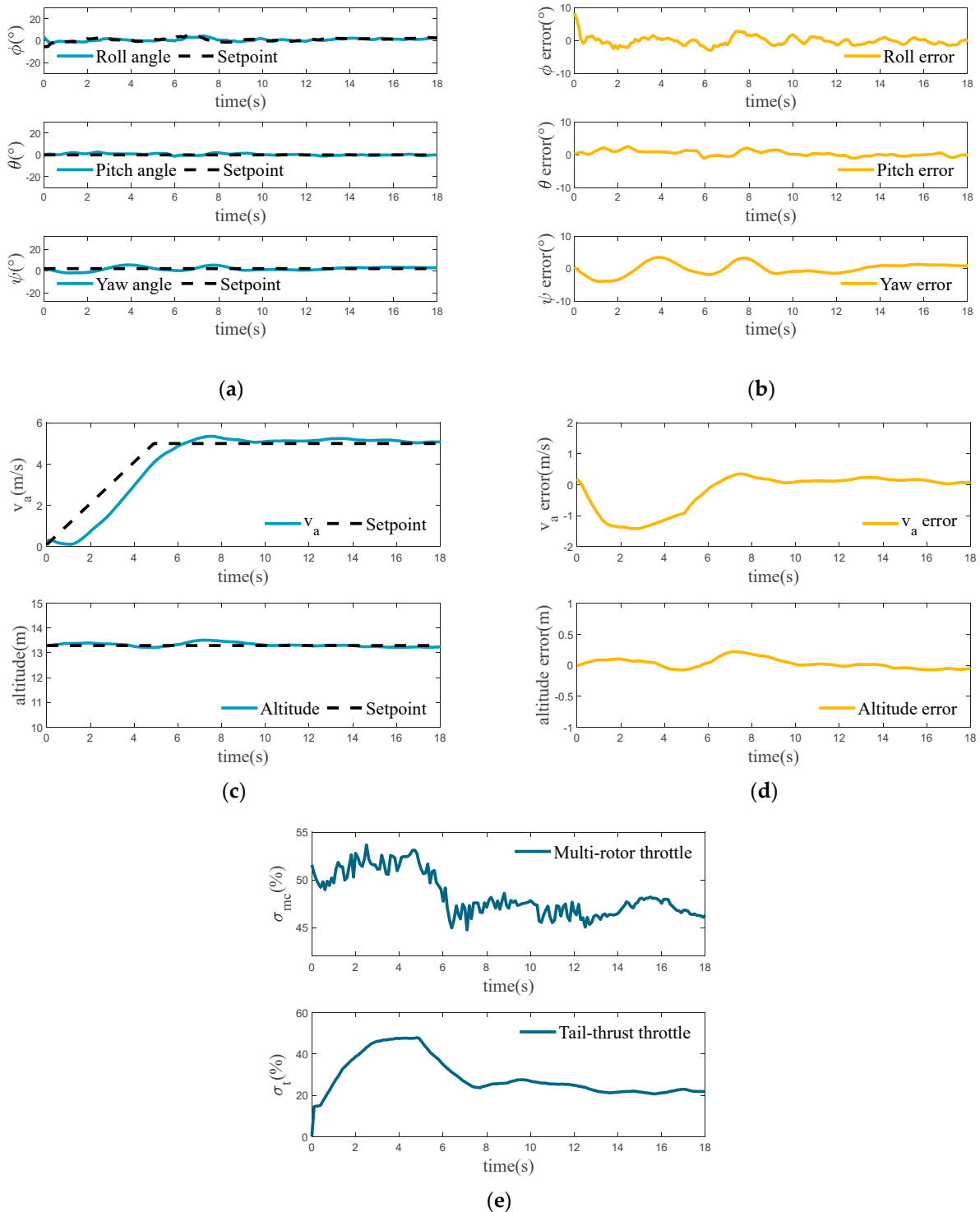


**Figure 15.** Experiment results for Case 1: (a) Attitude; (b) Attitude error; (c) Airspeed and altitude; (d) Airspeed and altitude error; (e) Multi-rotor and tail-thrust throttle.

Case 2: Vertical Motion

In this case, the drone adjusts its vertical velocity while maintaining its current forward velocity. The experimental results are presented in Figure 16. The drone’s attitude angle remains stable throughout the process, with only minor fluctuations. It is worth mentioning that, when the drone has an upward flight velocity, the aerodynamic forces apply a sustained torque on the fuselage to keep it head down, causing the drone to always have a slight downward pitch angle, but with minimal effect on the flight. Since the drone experiences a vertical velocity change, at which point the altitude is unlocked, only the desired vertical velocity tracking is performed here. The effectiveness of the drone’s ability to track vertical velocity changes in hybrid mode is evident. As the drone moves vertically, the direction of incoming airflow changes, causing the airspeed to fluctuate and, consequently, the forward flight velocity of the drone.

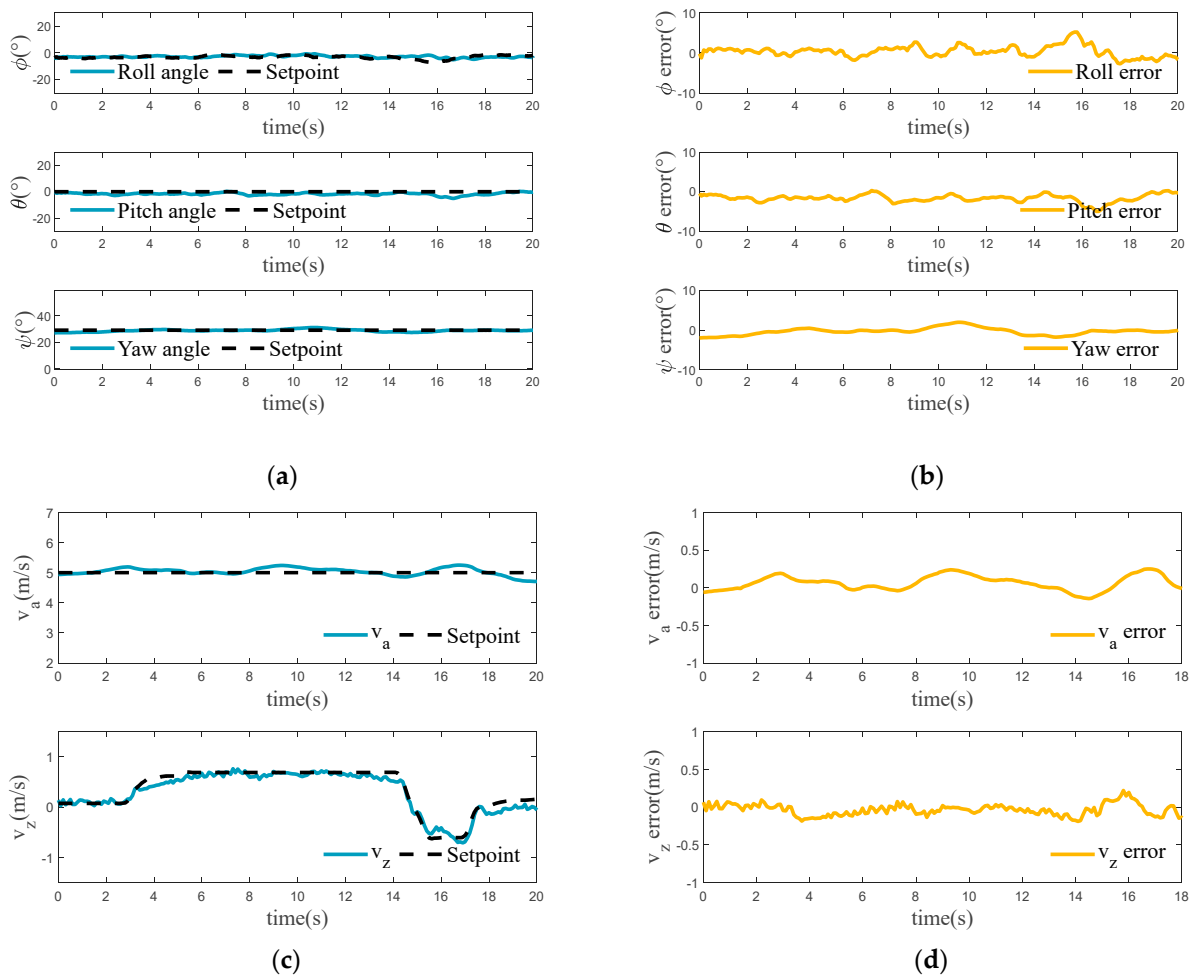
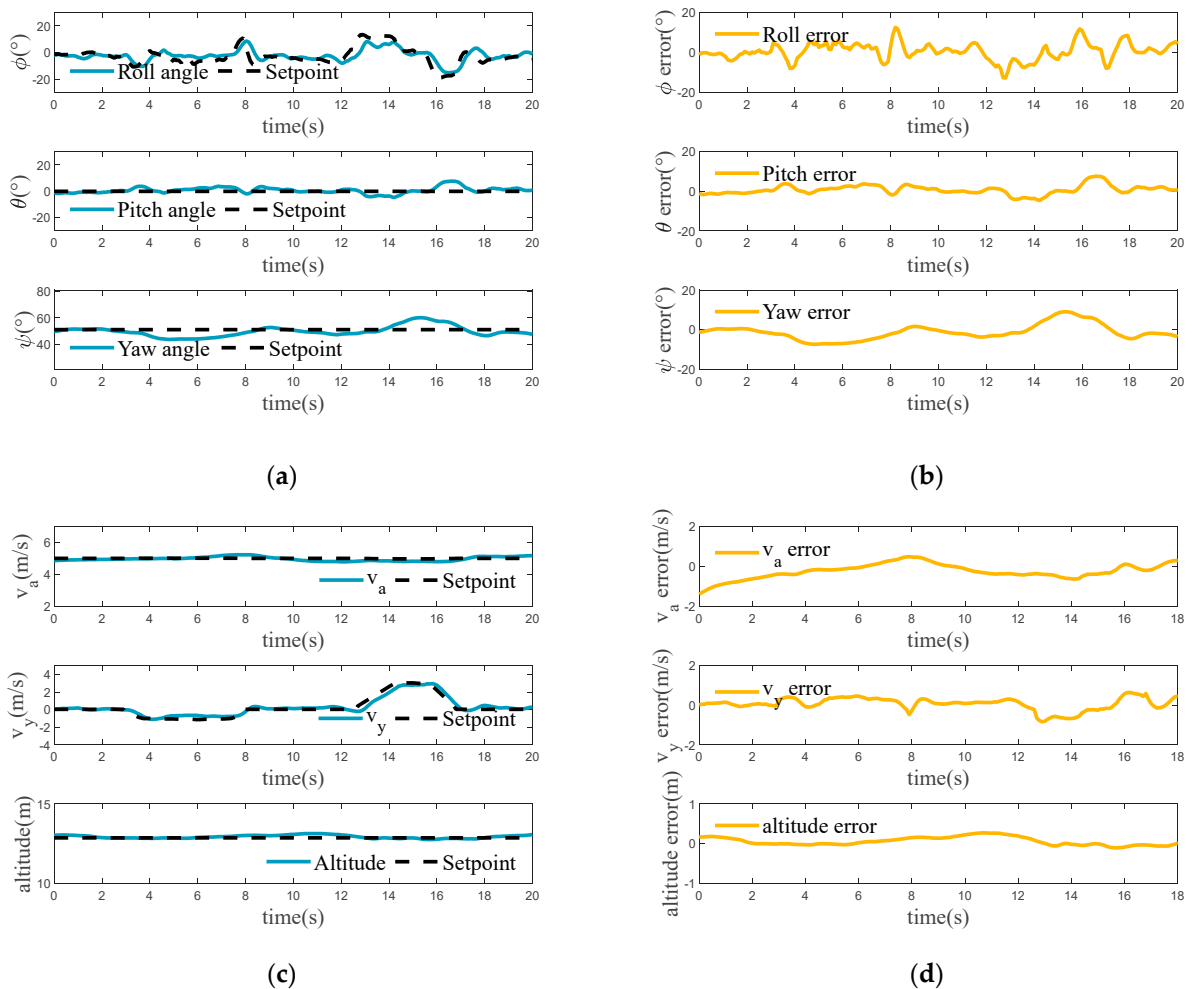


Figure 16. Experiment results for Case 2: (a) Attitude; (b) Attitude error; (c) Airspeed and vertical velocity; (d) Airspeed and vertical velocity error.

Case 3: Lateral Motion

The drone in this case will have a desired lateral flight velocity in hybrid mode flight, and the results are shown in Figure 17. The experimental results demonstrate that the drone effectively tracks the required roll angle for controlling the lateral flight velocity. However, there is a significant deviation in the yaw angle during this period due to the coupling of the drone’s roll and yaw. During this period, the aerodynamic changes are more drastic, which has a considerable effect on the pitch angle. Overall, the drone’s attitude change

remains within a relatively safe range. The forward velocity and altitude of the drone also fluctuate slightly as a result of the disturbance but remain relatively stable overall.



**Figure 17.** Experiment results for Case 3: (a) Attitude; (b) Attitude error; (c) Airspeed, lateral velocity, and altitude; (d) Airspeed, lateral velocity and altitude error.

#### Case 4: Yaw Motion

In this case, the yaw angle of the drone is altered during the flight. The experimental results in Figure 18 illustrate that the yaw angle of the drone can be precisely controlled in hybrid mode. Although the coupling characteristics cause some deviation in the roll angle during yaw angle changes, the effect is less critical than for lateral motion. The pitch angle also varies as a result of the disturbance, but the impact is also relatively minor. The forward flight velocity of the drone exhibits an obvious error due to the constant variation in the incoming flow caused by changes in yaw angle. This significantly affects the accuracy of the flight velocity. The drone's altitude remained stable throughout this period, and the fluctuations shown in the figure are due to airflow interference.

From the experimental results of the above cases, it can be concluded that the drone can meet the requirements of various motions during its hybrid mode flight, and the flight error is kept within a stable range. This indicates that the designed controllers and control strategy effectively implement the control of the drone's hybrid mode flight and can satisfy the control requirements in the face of actual flight situations and changes in airflow.

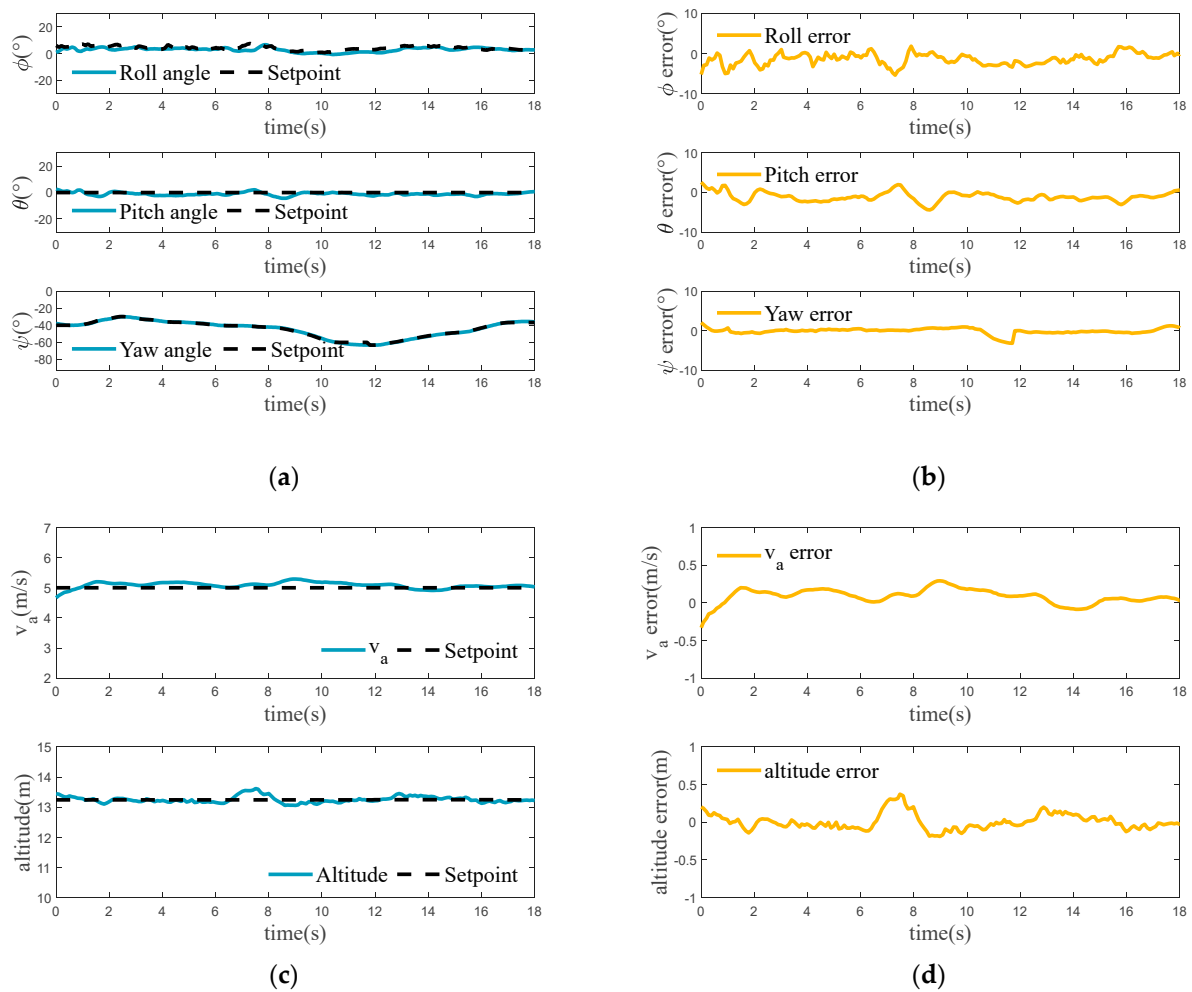


**Figure 18.** Experiment results for Case 4: (a) Attitude; (b) Attitude error; (c) Airspeed and altitude; (d) Airspeed and altitude error.

### 5.5. Energy Consumption

In hybrid mode, the lift of the fixed-wing reduces the lift required from the multi-rotor actuators. This undoubtedly reduces the battery's energy consumption to some extent. We measure the drone's energy consumption within the flight velocity envelope of hybrid mode. The flight velocity is set at 1 m/s intervals, and the energy consumption is recorded after the velocity has stabilized. The average value is calculated from several experiments. To compare with the flight energy consumption in multi-rotor mode, we conduct the experiment in multi-rotor mode in the same way and under the same conditions. The maximum velocity of this drone in multi-rotor mode is 6 m/s. The flight energy consumption in fixed-wing mode cannot be compared here because the drone's minimum flight velocity in fixed-wing mode exceeds 9 m/s, making it unable to maintain flight status within the hybrid mode's velocity envelope. Due to the high energy consumption of multi-rotor flight, it is almost certain that flying at cruising speed in fixed-wing mode will consume less energy than in hybrid mode, so fixed-wing mode energy consumption is not discussed here. The experimental result is shown in Figure 19.

When the flight velocity is below 3 m/s, the reduction in output from the multi-rotor actuators is not appreciable due to the low lift of the fixed-wing. However, due to the effect of aerodynamic forces and the activation of the tail-thrust actuator, the drone requires more energy compared to multi-rotor mode. As the flight velocity and the fixed-wing lift increase, the energy consumption in hybrid mode decreases significantly. In contrast, the higher the flight velocity in multi-rotor mode, the higher the required pitch angle of the

drone (as well as the significant aerodynamic drag of the fuselage and wings), resulting in a significant increase in the drone's energy consumption. Therefore, flying in hybrid mode can reduce the energy consumption of this drone within a specific flight velocity range.

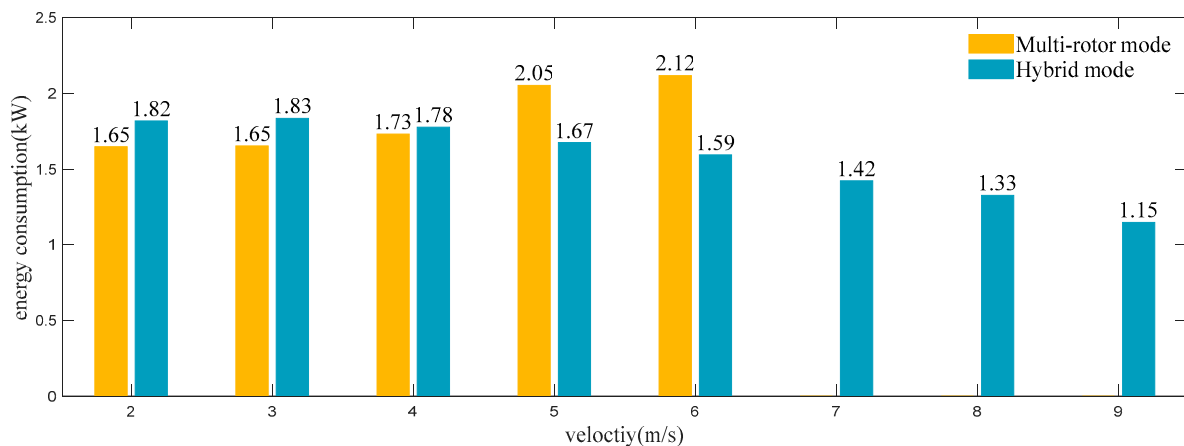


**Figure 19.** Energy consumption at different velocity.

## 6. Conclusions and Future Work

This paper proposes the addition of a third common flight mode (hybrid mode) to compound VTOL drones. The hybrid mode routinizes the transition mode and extends the range of flight velocities and potential applications for this type of drone. We have built a detailed dynamics model for the motion characteristics of hybrid mode and designed a control strategy for this mode. Additionally, we have designed anti-saturation PID controllers for altitude, velocity, and attitude control to counteract aerodynamic disturbances. Furthermore, this study identifies the parameters of the drone's fixed-wing lift and the thrust of the multi-rotor actuators to ensure accurate altitude control in hybrid mode. The feasibility of the control method has been verified through Gazebo simulation. A prototype has been built for real flight experiments, and the experimental results show that the control of hybrid mode flight can be effectively implemented and can meet the control requirements in actual flight situations. Finally, it has been proven that the use of hybrid mode flight can reduce the energy consumption of this type of drone during low-speed flight to some extent.

The next steps in the work are to improve the controllers used in hybrid mode to enhance the control of the drone. To enhance the control effectiveness, it may be worth considering incorporating a drone's control surfaces into the control process. Moreover, hybrid mode will be implemented as a common mode for decision-making and path planning in drone missions.

**Author Contributions:** Conceptualization, J.H. and Z.Q.; methodology, J.H. and X.Y.; software, J.H.; validation, J.H. and X.Y.; formal analysis, J.H.; investigation, J.H. and X.Y.; resources, K.L. and J.W.; data curation, J.H.; writing—original draft preparation, J.H.; writing—review and editing, J.H., J.W., Z.Q. and M.C.; visualization, J.H.; supervision, K.L. and J.W.; project administration, K.L. and J.W.; funding acquisition, K.L. and J.W. All authors have read and agreed to the published version of the manuscript.

**Funding:** This work was supported by Shenzhen Science and Technology Program under Grant JCYJ20200109142205924 and GXWD20201231165807008 (Corresponding author: Kun Liu).

**Data Availability Statement:** Datasets, photos, programs, and 3-D model files in this study are available upon correspondence with the first author.

**Conflicts of Interest:** The authors declare no conflict of interest.

## References

1. Mohsan, S.A.H.; Khan, M.A.; Noor, F.; Ullah, I.; Alsharif, M.H. Towards the Unmanned Aerial Vehicles (UAVs): A Comprehensive Review. *Drones* **2022**, *6*, 147. [[CrossRef](#)]
2. Idrissi, M.; Salami, M.; Annaz, F. A Review of Quadrotor Unmanned Aerial Vehicles: Applications, Architectural Design and Control Algorithms. *J. Intell. Robot. Syst.* **2022**, *104*, 22. [[CrossRef](#)]
3. Saeed, A.S.; Younes, A.B.; Cai, C.X.; Cai, G.W. A survey of hybrid Unmanned Aerial Vehicles. *Prog. Aerosp. Sci.* **2018**, *98*, 91–105. [[CrossRef](#)]
4. Ducard, G.J.J.; Allenspach, M. Review of designs and flight control techniques of hybrid and convertible VTOL UAVs. *Aerosp. Sci. Technol.* **2021**, *118*, 107035. [[CrossRef](#)]
5. Zhou, Y.M.; Zhao, H.R.; Liu, Y.L. An evaluative review of the VTOL technologies for unmanned and manned aerial vehicles. *Comput. Commun.* **2020**, *149*, 356–369. [[CrossRef](#)]
6. Saeed, A.S.; Younes, A.B.; Islam, S.; Dias, J.; Seneviratne, L.; Cai, G.W. A Review on the Platform Design, Dynamic Modeling and Control of Hybrid UAVs. In Proceedings of the International Conference on Unmanned Aircraft Systems (ICUAS), Denver, CO, USA, 9–12 June 2015; pp. 806–815.
7. Flores, G.; Lugo, I.; Lozano, R. 6-DOF Hovering Controller Design of the Quad Tiltrotor Aircraft: Simulations and Experiments. In Proceedings of the 53rd IEEE Annual Conference on Decision and Control (CDC), Los Angeles, CA, USA, 15–17 December 2014; pp. 6123–6128.
8. Park, S.; Bae, J.; Kim, Y.; Kim, S. Fault tolerant flight control system for the tilt-rotor UAV. *J. Frankl. Inst. Eng. Appl. Math.* **2013**, *350*, 2535–2559. [[CrossRef](#)]
9. Cetinsoy, E.; Dikyay, S.; Hancer, C.; Oner, K.T.; Sirimoglu, E.; Unel, M.; Aksit, M.F. Design and construction of a novel quad tilt-wing UAV. *Mechatronics* **2012**, *22*, 723–745. [[CrossRef](#)]
10. Muraoka, K.; Okada, N.; Kubo, D. Quad Tilt Wing VTOL UAV: Aerodynamic Characteristics and Prototype Flight. In Proceedings of the AIAA Infotech@Aerospace Conference, Seattle, DC, USA, 6–9 April 2009.
11. Lyu, X.; Gu, H.; Wang, Y.; Li, Z.; Shen, S.; Zhang, F. Design and implementation of a quadrotor tail-sitter VTOL UAV. In Proceedings of the 2017 IEEE International Conference on Robotics and Automation (ICRA), Singapore, 29 May–3 June 2017; pp. 3924–3930.
12. Verling, S.; Weibel, B.; Boosfeld, M.; Alexis, K.; Burri, M.; Siegwart, K. Full Attitude Control of a VTOL Tailsitter UAV. In Proceedings of the IEEE International Conference on Robotics and Automation (ICRA), Stockholm, Sweden, 16–21 May 2016; pp. 3006–3012.
13. Kai, J.-M. Full-Envelope Flight Control and a Transition Strategy for Compound eVTOL aircrafts. *arXiv* **2023**, arXiv:2312.09629.
14. Gu, H.W.; Lyu, X.M.; Li, Z.X.; Shen, S.J.; Zhang, F. Development and Experimental Verification of a Hybrid Vertical Take-Off and Landing (VTOL) Unmanned Aerial Vehicle(UAV). In Proceedings of the International Conference on Unmanned Aircraft Systems (ICUAS), Miami, FL, USA, 13–16 June 2017; pp. 160–169.
15. Wang, B.; Zhu, D.H.; Han, L.Y.; Gao, H.G.; Gao, Z.H.; Zhang, Y.M. Adaptive Fault-Tolerant Control of a Hybrid Canard Rotor/Wing UAV Under Transition Flight Subject to Actuator Faults and Model Uncertainties. *IEEE Trans. Aerosp. Electron. Syst.* **2023**, *59*, 4559–4574. [[CrossRef](#)]
16. Sato, M.; Muraoka, K. Flight Controller Design and Demonstration of Quad-Tilt-Wing Unmanned Aerial Vehicle. *J. Guid. Control. Dyn.* **2015**, *38*, 1071–1082. [[CrossRef](#)]
17. Liu, Z.; Theilliol, D.; Yang, L.Y.; He, Y.Q.; Han, J.D. Mode Transition and Fault Tolerant Control under Rotor-tilt Axle Stuck Fault of Quad-TRUAV. In Proceedings of the 10th International-Federation-of-Automatic-Control (IFAC) Symposium on Fault Detection, Supervision and Safety for Technical Processes (SAFEPROCESS), Warsaw, Poland, 29–31 August 2018; pp. 991–997.
18. Rohr, D.; Studiger, M.; Stastny, T.; Lawrance, N.; Siegwart, R. Nonlinear Model Predictive Velocity Control of a VTOL Tiltwing UAV. *IEEE Robot. Autom. Lett.* **2021**, *6*, 5776–5783. [[CrossRef](#)]
19. Oosedo, A.; Abiko, S.; Konno, A.; Uchiyama, M. Optimal transition from hovering to level-flight of a quadrotor tail-sitter UAV. *Auton. Robot.* **2017**, *41*, 1143–1159. [[CrossRef](#)]
20. Apkarian, J. Attitude Control of Pitch-Decoupled VTOL Fixed Wing Tiltrotor. In Proceedings of the International Conference on Unmanned Aircraft Systems (Icuas), Dallas, TX, USA, 12–15 June 2018; pp. 195–201.
21. Dai, C.; Bai, H.H.; Zeng, J.P. Nonlinear Stabilization Control of Tilt Rotor UAV During Transition Flight Based on HOSVD. In Proceedings of the IEEE Chinese Guidance, Navigation and Control Conference (CGNCC), Nanjing, China, 12–14 August 2016; pp. 154–159.
22. Qiao, Z.; Wang, D.; Xu, J.H.; Pei, X.B.; Su, W.; Wang, D.; Bai, Y. A Comprehensive Design and Experiment of a Biplane Quadrotor Tail-Sitter UAV. *Drones* **2023**, *7*, 292. [[CrossRef](#)]
23. Yu, Z.; Zhang, J.; Wang, X. Thrust Vectoring Control of a Novel Tilt-Rotor UAV Based on Backstepping Sliding Model Method. *Sensors* **2023**, *23*, 574. [[CrossRef](#)] [[PubMed](#)]
24. Yih Tang, Y.; Liu, H.H.T. Transition Control of a Tilt-Rotor VTOL UAV. In Proceedings of the 2018 AIAA Guidance, Navigation, and Control Conference, Kissimmee, FL, USA, 8–12 January 2018; pp. 1–15.
25. Liu, Z.C.; Guo, J.; Li, M.T.; Tang, S.J.; Wang, X. VTOL UAV Transition Maneuver Using Incremental Nonlinear Dynamic Inversion. *Int. J. Aerosp. Eng.* **2018**, *2018*, 6315856. [[CrossRef](#)]

26. Zhao, H.M.; Wang, B.; Shen, Y.Y.; Zhang, Y.N.; Li, N.; Gao, Z.H. Development of Multimode Flight Transition Strategy for Tilt-Rotor VTOL UAVs. *Drones* **2023**, *7*, 580. [[CrossRef](#)]
27. Yuksek, B.; Inalhan, G. Transition Flight Control System Design for Fixed-Wing VTOL UAV: A Reinforcement Learning Approach. In Proceedings of the AIAA SCITECH 2022 Forum, San Diego, CA, USA, 3–7 January 2022.
28. Dickeson, J.J.; Miles, D.; Cifdaloz, O.; Wells, V.L.; Rodriguez, A.A. Robust LPV  $H_\infty$  gain-scheduled hover-to-cruise conversion for a tilt-wing rotorcraft in the presence of CG variations. In Proceedings of the 26th American Control Conference, New York, NY, USA, 9–13 July 2007; pp. 5266–5271.
29. Ye, Z.; Chen, Y.L.; Cai, P.C.; Lyu, H.T.; Gong, Z.; Wu, J. Control Design for Soft Transition for Landing Preparation of Light Compound-Wing Unmanned Aerial Vehicles Based on Incremental Nonlinear Dynamic Inversion. *Appl. Sci.* **2023**, *13*, 12225. [[CrossRef](#)]
30. Kikumoto, C.; Urakubo, T.; Sabe, K.; Hazama, Y. Back-Transition Control with Large Deceleration for a Dual Propulsion VTOL UAV Based on Its Maneuverability. *IEEE Robot. Autom. Lett.* **2022**, *7*, 11697–11704. [[CrossRef](#)]
31. PX4 Dev Team. PX4 Autopilot User Guide (v1.11.0). Available online: <https://docs.px4.io/v1.11/en/> (accessed on 28 January 2024).
32. The MathWorks, Inc. Curve Fitting Toolbox—MATLAB. Available online: [https://www.mathworks.com/products/curvefitting.html?s\\_tid=srchtitle\\_Curve%20Fitting%20Toolbox\\_2](https://www.mathworks.com/products/curvefitting.html?s_tid=srchtitle_Curve%20Fitting%20Toolbox_2) (accessed on 28 January 2024).

**Disclaimer/Publisher’s Note:** The statements, opinions and data contained in all publications are solely those of the individual author(s) and contributor(s) and not of MDPI and/or the editor(s). MDPI and/or the editor(s) disclaim responsibility for any injury to people or property resulting from any ideas, methods, instructions or products referred to in the content.